EXTENDING THE LOW FREQUENCY ACOUSTIC CENTRE CONCEPT TO DIRECTIONAL LOUDSPEAKERS

JA Hargreaves Acoustics Research Centre, University of Salford, UK

1 INTRODUCTION

The Acoustic Centre (AC) of a loudspeaker is an oft discussed property, especially when considering the geometrical point of rotation for polar or balloon measurements. It is defined in ANSI S1.1-2004 as “the position of the virtual point source from which sound pressure varies inversely [with] distance” and in IEC 61094-3-2016 as “the point from which […] spherical wavefronts […] appear to diverge”.

This seemingly simple definition has, however, proven surprisingly slippery and difficult to apply in a quantified way to a broad range of sources over a wide frequency range. When applied to loudspeakers, the literature can largely be split as attempting to explain either low or high frequency AC trends, though some rather causal discussion conflating one with the other also appears.

At low frequencies, wavelength is much larger than cabinet size and radiation close to omnidirectional. Mathematically, one is therefore considering a source that is almost exactly equivalent to a monopole. This area of study for loudspeakers stems mainly from the ideas of Vanderkooy[1]. It acknowledges that higher-order directivity terms may exist, but only considers the dipole term to potentially be significant. Thus, it focuses on finding an AC that zeroes that, leaving a pure monopole. Vanderkooy’s 2006 paper presents some quite sophisticated theory but only demonstrates a relatively simple measurement approach based on the pressure at two positions. A recent paper by Bellow and Leishman[2] closes that gap by defining AC based on ‘dipole-to-monopole moment ratio’, which allows Vanderkooy’s concept to be tested more rigorously on a set of theoretical source problems and applied to a measured test case. Closely related ideas appear in literature on microphone calibration (see review in ref. 2) but the small transducer size there means they apply to much higher frequencies.

For loudspeakers at higher frequencies, geometric of features of the cabinet (e.g., loudspeaker cones and/or horns) become large with respect to wavelength and can achieve significant pattern control. Radiation here can be far from omnidirectional, yet at sufficient distance from the loudspeaker the wavefronts are still spherical, and pressure still decays inversely with distance. This is a key difference with the low frequency methods above: they are designed to be applied in the nearfield but at high frequencies quasi-far-field measurement is assumed. The setting of AC at high frequencies appears to mainly be done quite empirically, with users often choosing it based on known transducer positions. But it is also clear that measuring based on a convenient point of rotation will produce incorrect results unless a complex, i.e., with phase, correction is employed[3].

To bridge this gap, a framework is required that spans both these paradigms. Bellow and Leishman[2] agree, stating that “the need remains for a more consistent definition of the acoustic centre, applying to all sources and generalizing to all frequencies”. As indicated above, this requires that an AC can be found for higher-order sources with non-monopole directionality. Vanderkooy[1] also acknowledged this limitation and wrote that his “low-frequency acoustic center concept does not apply to loudspeakers that have a purely dipolar or cardioid-like polar pattern […, since] no choice of origin can make such a transducer omnidirectional”. He also noted that “for a [dipole] loudspeaker, […] it is perhaps possible to define an origin which reduces the quadrupole term to zero, so that its dipole character is clearer […; an] acoustic dipole center. This rather esoteric concept is not pursued any further”. This paper explores these concepts – including cardioid loudspeaker optimisation – and will show “esoteric” results such as optimal acoustic centres for dipole and/or multipole expansion.

1.1 Spherical Harmonic and Spherical Basis Functions

A framework that unites both these frequency ranges is the increasingly prevalent one based on Spherical Harmonic (SH) functions. This was first suggested for loudspeaker balloon measurements by Angus and Evans in 1998[4], but has been cemented into the loudspeaker measurement psyche more recently due to it being the basis of the 'holographic' nearfield measurement approach used by the Klippel Near Field Scanner[5]. Notably, this allows the separation of incoming and outgoing sound, hence measurements are possible in non-anechoic environments (subject to conditions). The SH framework has also gained popularity due to its compatibility with virtual acoustic simulations[6–9].

On a sphere, SH functions form an orthogonal set equivalent to the harmonic terms used in a Fourier series. They are, therefore, an effective way of interpolating and/or encoding loudspeaker balloon data, as Angus and Evans suggested[4]. But because the acoustic waves must satisfy the Helmholtz equation, the radial function can be deduced from the angular SH function and the wavenumber, leading to what are sometimes called Spherical Basis (SB) functions in the literature[9]. These are rather more powerful, since they are what allows incoming and outgoing sound to be separated[5,10]. They are also highly compatible with current approaches in loudspeaker measurement because the radial functions become a scaled version of a monopole in the high frequency or far-field limit. Thus, the 'complex point source' model[11] is simply a far-field approximation to the SB framework.

SB functions have additionally been shown to satisfy further orthogonality conditions when utilised with a metric called 'cross-intensity'[12,13]. Notably, these apply over a surface of arbitrary shape, debunking the common misconception that SH data can only be measured with spherical microphone arrays. This does, however, require surface-normal particle velocity or pressure gradient data, which is only available with intensity probes. It is used herein to obtain SB coefficients. Note that the Klippel Near Field Scanner[5] already allows measurement in non-spherical regions (the ones it uses are believed to typically be closer to cylindrical) but this is achieved via numerical matrix inversion. In contrast, the method used herein is a forward method based on orthogonality with no matrix inversion required. But even if an algorithm involving matrix inversion is chosen (this does, for example, give increased flexibility over measurement positions), it is anticipated that the orthogonality property in ref. 12 should be able to inform signal processing schemes that improve matrix conditioning.

The SB representation displays the trend exploited by Vanderkooy[1] and Bellow and Leishman[2] for monopoles, that translation to a sub-optimal expansion point (AC) creates additional components of higher orders[6,7]. Klippel *et al*[5] discuss how an accurate AC is required to have the SB coefficients converge sufficiently to give acceptable accuracy, and implement an adaptive adjustment to find this. These properties of the SB expansion naturally suggest the following definition for the AC:

> *The Acoustics Centre is the point at which the Spherical Basis function coefficients converge most rapidly with respect to source order, or which gives minimum error for a fixed source order.*

This definition naturally extends the AC concept to directional loudspeakers, since one can search for an AC that optimally captures the directionality of the sound source under test without bringing in higher orders of SB functions unnecessarily just to explain translation relative to a sub-optimal expansion point. This idea has already seen some exploration in the literature, e.g., in refs. 6–8, there motivated by finding the AC that allows optimal encoding of measured musical instrument directivities.

The word "search" here is a disadvantage of the SH-based approach. A key advantage of the method of Vanderkooy[1] and the more recent extension by Bellow and Leishman[2] is that, by restricting the analysis to zeroth and first order terms, a closed-form expression can be found to compute the AC from measurements at other positions. It is notable that ref. 2 does include a section on SB functions, but this is only to incorporate them into their monopole / dipole moment framework and remains limited to centring monopoles. Once the AC concept is extended beyond this zeroth order, closed form expressions are not forthcoming, and a numerical search becomes necessary. Bellow and Leishman[2] suggest that this is computationally expensive, though in the research herein it was mostly not seen to be; certainly it was insignificant compared to the time and effort required to measure such datasets

in the first place. A bigger issue is whether the search finds the global minimum. Shabtai and Vorländer[8] state that the search space is 'convex' – and therefore ideal for standard optimisers such as 'steepest descent' – only when "employed on sources with low-order radiation patterns". Similar results to this were found herein, and random restarts were used to mitigate the effect where seen.

Choice also arises over what metric should be minimised by the search. The majority have worked directly from the set of encoded SB coefficient via 'centre of mass' type statements[7], though Deboy and Zotter[6] and Shabtai and Vorländer[8] also proposed statements that aim to discriminate based on the phase of the reconstructed pressure field. This paper differs in that it uses metrics based on the residual of the sound field reconstructed from the SB coefficients, compared to the original measured data. In the infinite order limit, this is equivalent to computing metrics directly on the SB coefficients. But when analysis is truncated to finite orders – as it always is in practice – there are differences. Essentially this approach studies convergence against a ground truth, whereas metrics based solely on SB coefficients only capture relative self-convergence. Since the measured ground truth data is available, this seems a good choice, though it does incur higher computational cost.

1.2 Paper Outline, Methodology, and Experimental Context

Section 2 reviews the spherical harmonic model of acoustic sources. Section 3 then presents the metrics that will be used for the AC search and characterises them on analytical multipoles. Section 4 applies this framework to a single driver sealed axisymmetric loudspeaker, investigating how the AC moves with frequency and the effect of an obstruction. Section 5 then considers the optimisation of a dual driver cardioid loudspeaker, finding the 1st order AC at each frequency that enables optimal cardioid directivity. Finally, section 6 draws conclusions and identifies avenues for future research.

The results presented in this paper are all simulated and use axisymmetric geometries, as was done by Vanderkooy[1]. A difference is that he used axisymmetric BEM whereas here axisymmetric FEM was employed, with a PML region beyond the radius of the measurement points. This choice was simply because the software used – COMSOL Multiphysics v6.1 – does not currently implement axisymmetric BEM; had it done then BEM would have been similarly suitable. Matlab LiveLink was used to extract data from COMSOL. This was postprocessed in Matlab and then returned to COMSOL either to produce AC position overlays or combine datasets, as was necessary in section 5.

Axisymmetric models are beneficial to use as a testbed as they are far more computationally efficient, since only a cross-section needs to be meshed. They also simplify the search process since the AC must lie on the axis of symmetry, hence z is the only unknown coordinate. This simplifies presentation of results too. Searches were performed that included an off-axis search space to validate that the algorithm converged to the correct on-axis position, but these are not included herein for brevity.

Furthermore, precise characterisation of axisymmetric loudspeakers is of genuine practical interest in sound field control applications. And when performing laboratory measurements or validating room acoustic models, precise knowledge of the incident field is required which in turn requires precise characterisation of the source[9]. The SB representation is the most compact way to do this, and the number of non-zero coefficients is square-rooted when the source is axisymmetric, compressing the source description and expediting translation and rotation operations.

For this reason, a prototype axisymmetric loudspeaker was designed and constructed. It is shown in fig. 1. The bass stage, which the simulated test case in section 5 is based on, features two 210mm diameter woofers in a 600mm long, 260mm diameter and 5mm thick Perspex tube, lined with wadding to damp resonances. The baffles and internal bracing structure are built from 18mm plywood. The two drivers share a common chamber due to the efficiency gains Cheer demonstrated this design to possess[14]. These are fed by separate amplifier channels, meaning any combination of monopole or dipole can be achieved. The rear plate is both for practicality of mounting and to discourage rearward directivity from that driver at higher frequencies. The objective in section 5 is to find the relative amplitude and phase of the drive signal to each loudspeaker to achieve optimal cardioid directivity.

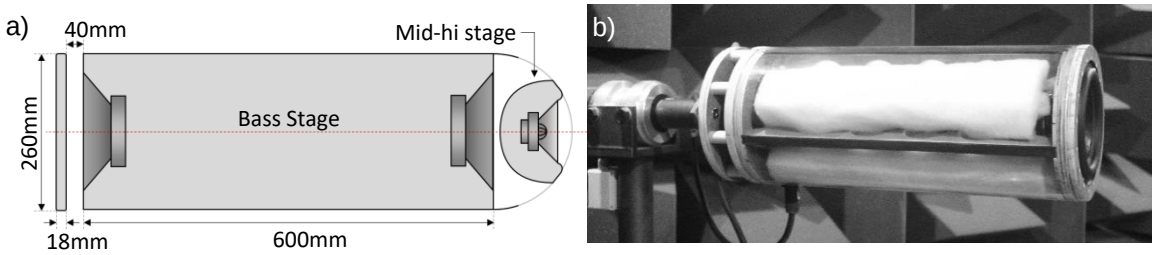

Figure 1: Prototype axisymmetric loudspeaker. a) Full concept including front mid-high stage. b) Bass-stage of prototype, as inspires the test case in section 5, in the University of Salford Acoustic Laboratory's anechoic chamber mounted on their Four Audio ELF measurement robot.

The front mid-hi stage is not considered in this paper but is of relevance since the vision was that it's AC might align with the AC of the bass stage at the crossover frequency, which is expected to be slightly in front of the front woofer at that frequency. Section 4 also investigates the effect of this obstruction on the AC of the bass stage, notably whether its presence moves the AC forward or back.

2 SPHERICAL HARMONIC AND BASIS MODEL FOR SOURCES

Consider an acoustic field radiating outwards from a time-harmonic source with frequency f Hz. This can be represented by a weighted sum of outgoing spherical basis functions $H_{m,n}^{\mathrm{out}}$ as:

$$p(\mathbf{r},\omega) = \sum_{n=0}^{\infty}\sum_{m=-n}^{n} b_{m,n}(\omega,\mathbf{r}_0)H_{m,n}^{\mathrm{out}}(\mathbf{r}-\mathbf{r}_0,\omega). \tag{1}$$

Here $p(\mathbf{x},\omega)$ is the complex (with phase) pressure amplitude at position $\mathbf{x}$ and angular frequency $\omega = 2\pi f$. $b_{m,n}$ is a set of coefficients that describe the radiation from the source and $\mathbf{r}_0$ is the expansion point, which in the context of this paper can be thought of as the trial AC. $H_{m,n}^{\mathrm{out}}$ is defined as:

$$H_{m,n}^{\mathrm{out}}(\mathbf{r}-\mathbf{r}_0,\omega) = Y_n^m(\beta,\alpha)h_n^{\mathrm{out}}(kr). \tag{2}$$

Here h_n^{out} is an outgoing spherical Hankel function, being a spherical Hankel function of the first kind if $\mathrm{e}^{-\mathrm{i}\omega t}$ time variation is assumed (or of the second kind if $\mathrm{e}^{+\mathrm{i}\omega t}$ is assumed). $k = \omega/c_0$ is wavenumber, with speed of sound c_0, and radius $r = |\mathbf{r}-\mathbf{r}_0|$. $Y_n^m(\beta,\alpha)$ is a spherical harmonic function defined as:

$$Y_n^m(\beta,\alpha) = (-1)^m\sqrt{\frac{(2n+1)}{4\pi}\frac{(n-|m|)!}{(n+|m|)!}}P_n^{|m|}(\cos\beta)\mathrm{e}^{\mathrm{i}m\alpha}. \tag{3}$$

Here P_n^m is an associated Legendre function. α and β are the azimuth and polar angles respectively, whose relationship to $\mathbf{r}$ and $\mathbf{r}_0$ is depicted in fig. 2. Note that all the simulations herein are performed in so called 'front-pole' orientation, that is, the loudspeaker points in the $+z$ direction where $\beta = 0$.

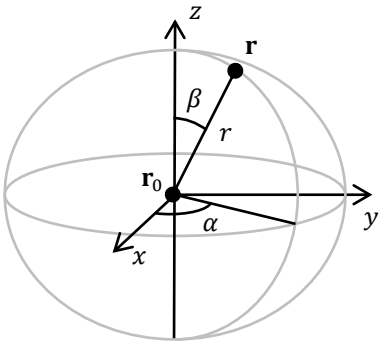

Figure 2: Coordinate System

Note that because the cases considered are all axisymmetric, all terms with $m \neq 0$ will have $b_{m,n} = 0$ and contribute nothing. All terms with $m \neq 0$ in eq. 3 therefore effectively vanish, so the pressure field p becomes independent of α, and $P_n^{|m|}(\cos\beta)$ is replaced by $P_n(\cos\beta)$, a much simpler Legendre polynomial. Notably $P_0(\cos\beta) = 1$ and $P_1(\cos\beta) = \cos\beta$, making it clear that $b_{0,0}$ is the monopole coefficient and $b_{0,1}$ is the dipole coefficient.

Extrapolating Vanderkooy's definition of low frequency AC from monopoles to order-limited sources with the form of eq. 1, the true AC for this frequency $\mathbf{r}_c(\omega)$ is defined as being the expansion point that leads to the lowest value N for which all $b_{m,n} = 0$ for $n > N$.

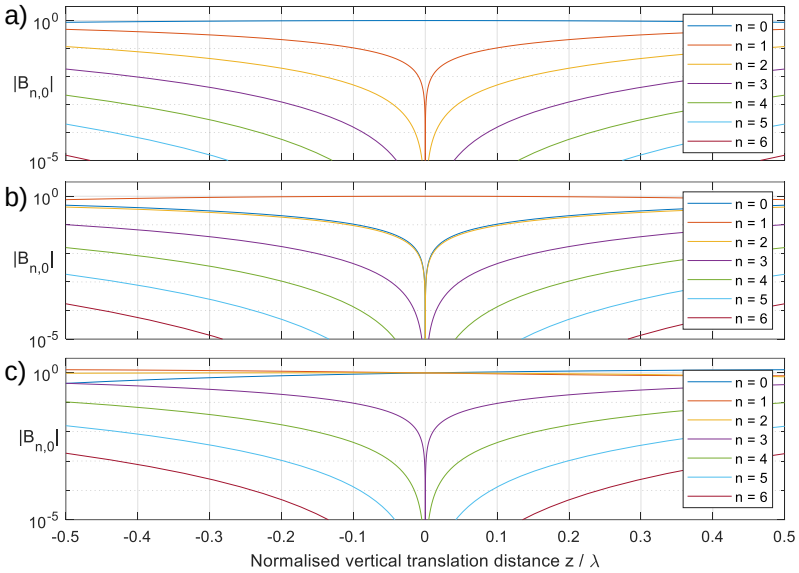

Figure 3: Effect of translation between expansion point and true AC on $b_{n,0}$ coefficients. a) monopole, b) dipole, c) 2nd order multipole.

As already mentioned, having $\mathbf{r}_0 \neq \mathbf{r}_c$ gives other coefficients more energy than necessary. Figure 3 shows this for three analytical source types. For the monopole (top), $b_{m,n} = 1$ for $m = n = 0$ and are 0 otherwise. At zero translation, this is seen in the reconstructed coefficients, but elsewhere all are used to explain the translation, gaining increasing amplitude as the translation increases. The dipole (middle) shows a similar trend except now it is the $n = 1$ curve that is constant, and the others – including the $n = 0$ curve – become significant only when translation is involved. Finally, the bottom plot shows a 2nd order multipole for which $b_{m,n} \neq 0$ only for $m = 0$ and $n \leq 2$. Those three curves remain significant everywhere, but the others are only significant once translation is involved. Looking at these it appears that the coefficients contain features – a defined minimum – that can be used to match the expansion point to the AC.

2.1 Encoding of measured data to spherical basis coefficients

The standard method for obtaining the SB coefficients $b_{m,n}$ is to measure pressure at a set of points over a sphere of radius r_{meas}. On this, the pressure field can be interpolated using SH functions and a set of coefficients $c_{m,n}$ as follows, which is the approach suggested by Angus and Evans[4] in 1998:

$$p(r_{\text{meas}}, \beta, \alpha, \omega) = \sum_{n=0}^{\infty} \sum_{m=-n}^{n} c_{m,n}(\omega, r_{\text{meas}}) Y_n^m(\beta, \alpha). \tag{4}$$

Here $c_{m,n}$ has been stated to a function of r_{meas} as well as ω, since the values obtained will depend on measurement radius. These coefficients can be found from the measured pressure field by:

$$c_{m,n}(\omega, r_{\text{meas}}) = \int_{-\pi}^{\pi} \int_{0}^{\pi} p(r_{\text{meas}}, \beta, \alpha, \omega) Y_n^m(\beta, \alpha)^* \sin\beta \, d\beta d\alpha. \tag{5}$$

Here the well-known SH orthogonality over a sphere property has been exploited. By comparing eq. 4 to eq. 1, it is evident that the radius-independent coefficients $b_{m,n}$ can be found from $c_{m,n}$ by:

$$b_{m,n}(\omega) = c_{m,n}(\omega, r_{\text{meas}}) / h_n^{\text{out}}(kr_{\text{meas}}). \tag{6}$$

The centre of expansion $\mathbf{r}_0$ is, however, locked to the geometric centre of the measurement sphere. To search for the AC, translations can be applied in the SB domain[7,9]. But this requires measuring with a far higher order than the source is expected to possess, since all the translational 'smudging' over SB order, as shown in Figure 3, must be captured. It is expected that the reverse translation will then have a 'sharpening' effect at the correct AC, if sufficiently high measurement order was used.

2.2 Method based on 'Cross-Intensity'

Limitations of the method above are that: i) the measurement points must be on a sphere, and ii) that the measurements must be performed in an anechoic environment. This latter restriction is often expected, but the success of the Klippel Near Field Scanner[5] has demonstrated that it is not essential.

The second restriction arises because the encoding in eq. 4, which is purely pressure-based, cannot discriminate between waves that are incoming and outgoing, hence room reflections cannot be removed. Adding co-located measurements of particle velocity – or equivalently, pressure gradient – allows discrimination between waves that are incoming and outgoing, hence avoids the issue. The version of this based on 'cross-intensity' and presented in ref. 12 is also valid for non-spherical measurement surfaces because it is derived via Green's theorem. It is most compactly stated as:

$$b_{m,n}(\omega) = -\mathrm{i}k \iint_S \left[p(\mathbf{r},\omega) \frac{\partial J^*_{m,n}}{\partial n}(\mathbf{r}-\mathbf{r}_0,\omega) - J^*_{m,n}(\mathbf{r}-\mathbf{r}_0,\omega) \frac{\partial p}{\partial n}(\mathbf{r},\omega) \right] dS. \tag{7}$$

Here S is the measurement surface and $J_{m,n}$ is a regular spherical basis function, which is defined the same as $H^{\mathrm{out}}_{m,n}$ in eq. 2 except that the radial function is a spherical Bessel function. $\partial/\partial n$ is shorthand for $\hat{\mathbf{n}} \cdot \nabla$, where $\hat{\mathbf{n}}$ is an inward-pointing unit vector that is normal to S at $\mathbf{r}$ and the gradient ∇ is taken with respect to $\mathbf{r}$. An asterisk indicates complex conjugation. With this statement, the user is also free to choose $\mathbf{r}_0$, hence an AC search can be performed with no translation operations necessary. If the measurement surface S is spherical, and $\mathbf{r}_0$ is at its centre, then this is equivalent to the 2010 method of Melon *et al*[10]. Note that in practice, all such boundary integrals, including the one in eq. 5, will be approximated by a set of point measurements that are appropriately weighted and then summed.

2.3 Far-Field Extrapolation

The radius r_{meas} at which measurements are taken in eq. 5 is typically rather arbitrary, usually being defined by the size of the measurement space available, and is unlikely to match the listening distance of interest. There is, therefore, a need for a radius-independent description of directivity. The $b_{m,n}$ coefficients give this, but in a form that is not familiar to most practitioners in the audio industry.

A solution is to look at directivity in the far-field limit. This is especially appropriate for concert sound use, where distances are great, and it is compatible with high-frequency AC concepts. It is defined:

$$p_{\mathrm{ff}}(\beta,\alpha,\omega) = \lim_{r\to\infty} \left[p(r,\beta,\alpha,\omega) \times \frac{4\pi r}{\mathrm{e}^{\mathrm{i}kr}} \right]. \tag{8}$$

Here the term $4\pi r/\mathrm{e}^{\mathrm{i}kr}$ compensates for the distance attenuation and delay experienced by a monopole at that distance, leading to a distance-independent quantity for sufficiently large r. It can be interpolated using SH functions and a set of coefficients $d_{m,n}$ as:

$$p_{\mathrm{ff}}(\beta,\alpha,\omega) = \sum_{n=0}^{\infty} \sum_{m=-n}^{n} d_{m,n}(\omega) Y^m_n(\beta,\alpha). \tag{9}$$

In eq. 1-3, terms with different n have difference order spherical Hankel functions $h^{\mathrm{out}}_n(kr)$. These decay differently with kr, in the nearfield (small kr) especially. But for large kr the 'large-argument' approximation $h^{\mathrm{out}}_n(kr) \approx \mathrm{i}^{-n} h^{\mathrm{out}}_0(kr)$ applies, where $h^{\mathrm{out}}_0(kr) = \mathrm{e}^{\mathrm{i}kr}/\mathrm{i}kr$ is a scaled version of a monopole. This means that if one is far enough away from source, and/or frequency is high enough, then all terms in its directivity decay at the rate a monopole would. This can be employed to give:

$$d_{m,n}(\omega) = \lim_{r\to\infty} \left[h^{\mathrm{out}}_n(kr) \times \frac{4\pi r}{\mathrm{e}^{\mathrm{i}kr}} \right] = \mathrm{i}^{-n} \frac{\mathrm{e}^{\mathrm{i}kr}}{\mathrm{i}kr} \frac{4\pi r}{\mathrm{e}^{\mathrm{i}kr}} \times b_{m,n}(\omega) = \frac{4\pi}{\mathrm{i}k} \mathrm{i}^{-n} b_{m,n}(\omega). \tag{10}$$

Fr-field pressure can also be computed directly from the measured data via a boundary integral equation, so long as particle velocity – or equivalently, pressure gradient, is known:

$$p_{\mathrm{ff}}(\hat{\mathbf{d}}) = -\mathrm{e}^{\mathrm{i}k\hat{\mathbf{d}}\cdot\mathbf{r}_0} \iint_S \mathrm{e}^{-\mathrm{i}k\hat{\mathbf{d}}\cdot\mathbf{r}} \left[\mathrm{i}k\hat{\mathbf{n}}\cdot\hat{\mathbf{d}}p(\mathbf{r}) + \frac{\partial p}{\partial n}(\mathbf{r})\right] d\mathbf{r}. \tag{11}$$

Here $\hat{\mathbf{d}}$ is a unit vector pointing in the direction of evaluation. Data computed this way will be used as the reference when calculating the reconstruction error in the far field.

3 ACOUSTIC CENTRE FOR THEORETICAL MULTIPOLES

In this section a 'measured' pressure field p_{M} is simulated using eq. 1 with its $b_{m,n}$ coefficients set to specific values. Eq. 7 is then used to recover those coefficients, but with a different trial AC $\mathbf{r}_0$, and the normalised error in the reconstructed pressure p_{R} is computed. Reconstruction error is quantified by the RMS of the residual $p_{\mathrm{M}} - p_{\mathrm{R}}$ normalised by the RMS of the ground truth pressure field p_{M}:

$$E\{p_{\mathrm{M}}, p_{\mathrm{R}}\} = \sqrt{\langle |p_{\mathrm{M}} - p_{\mathrm{R}}|^2\rangle / \langle |p_{\mathrm{M}}|^2\rangle}. \tag{12}$$

Here $\langle \cdots \rangle$ is shorthand for a boundary integral of a quantity over S, as was seen in eq. 7 and 11. The metric is computed at r_{meas} by comparing p_{M} with p_{R} computed using eq. 1. It is also computed for far field pressure by comparing eq. 11 applied to p_{M} with $p_{\mathrm{ff,R}}$ from eq. 9. r_{meas} was set to 0.9m and pressure and its gradient were computed every 3°; these settings are used in all subsequent simulations too. Additionally, and here only, -40dB Gaussian 'measurement noise' was added.

Figure 4 shows the results for a source with a true AC $\mathbf{r}_{\mathrm{c}} = [0, 0, 0.2]$. It is a dipole so $b_{0,1} = 1$ and all other $b_{m,n} = 0$. The trial AC $\mathbf{r}_0$ was varied in the z direction and the reconstruction error is plotted for both the measurement radius and in the far field. The $n = 0$ AC does not converge in either case because it – being omnidirectional – cannot capture the dipole behaviour. The $n = 1$ trend, in contrast, shows a distinct error minimum at the correct AC, which is encourages its use as a search metric. Higher order behaviour varies between near and far field pressure, with the former plateauing to form ever wider valleys, while the latter converges further but with minima sometimes different to the true AC. The latter is thought to be due to overfitting of the far field reconstruction compute using eq. 11, making this a less useful search metric. Pressure at the measurement radius was therefore chosen as the metric for the single driver loudspeaker test case in section 4. From this a further metric was

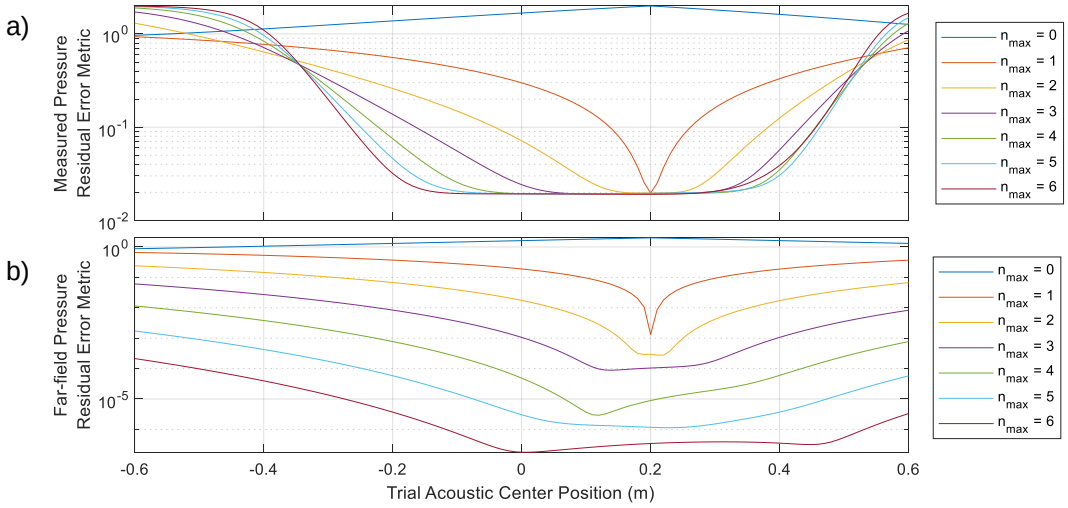

Figure 4: Normalised reconstruction error for a 100 Hz dipole at $z = 0.2\mathrm{m}$ for 'measured' pressure at $r_{\mathrm{meas}} = 0.9\mathrm{m}$ (top) and far field pressure (bottom), at various reconstruction orders n.

developed that can find both sound AC and order, but there is insufficient space here to report this. Far field pressure is used in the latter part of section 5 because far field directivity is the focus there.

4 ACOUSTIC CENTRE FOR AN AXISYMMETRIC SINGLE DRIVER SEALED CABINET LOUDSPEAKER

This first test case is based on half of the loudspeaker described in section 1.2 and shown in fig. 1. It is 260mm diameter and 300mm deep, centred with its front baffle at $z = 0\text{m}$ in a 1m radius air volume bounded by a 0.25m thick Perfectly Matched Layer (PML), which has a scaling factor of 0.5 and a scaling curvature parameter of 2. These PML parameters are used in section 5 too.

The geometry is shown in fig. 5. The radial slice modelled in COMSOL was only the right half of this – all plots have been mirrored for ease of interpretation. The maximum element size was 0.6mm, allowing $\lambda/5$ meshing up to 10kHz, though results here are only shown up to 2.5kHz. An optional obstruction is included, to show the effect the coaxial mid-hi stage in fig. 1a would have on the AC.

The metric in eq. 12 is evaluated at the measurement radius $r_{\text{meas}} = 0.9\text{m}$, as per fig. 4a. The trial AC with the minimum metric value was found using a bounded version of Matlab's built-in `fminsearch` function[15].

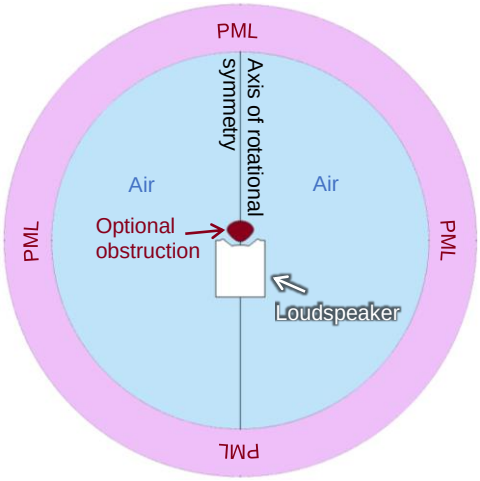

Figure 5: Geometry of single driver loudspeaker model

Figure 6 shows the minimum value of the metric, and the z coordinate of the trial AC that gave it, versus frequency. It can be seen that the monopole term captures the majority of the behaviour up to 200Hz. Above that the dipole term becomes significant, and then higher order terms from 400Hz. The error metric is shown for $0 \leq n \leq 5$ but the optimal trial AC is only shown for $0 \leq n \leq 2$ since for $n > 2$ the AC result is very erratic due to the search space being non-convex and having multiple minima, as found by Shabtai and Vorländer[8]. The obstruction has very little effect on error arising from only using the monopole term, though it shifts the zeroth-order AC back by 1.39cm on average. It's presence (dashed lines) has a stronger effect on the higher-order terms, and more need to be brought in at a lower frequency to explain its effect. But this is all above 300Hz, which is the intended crossover frequency with the mid-hi stage in the real prototype, hence is not an issue for that.

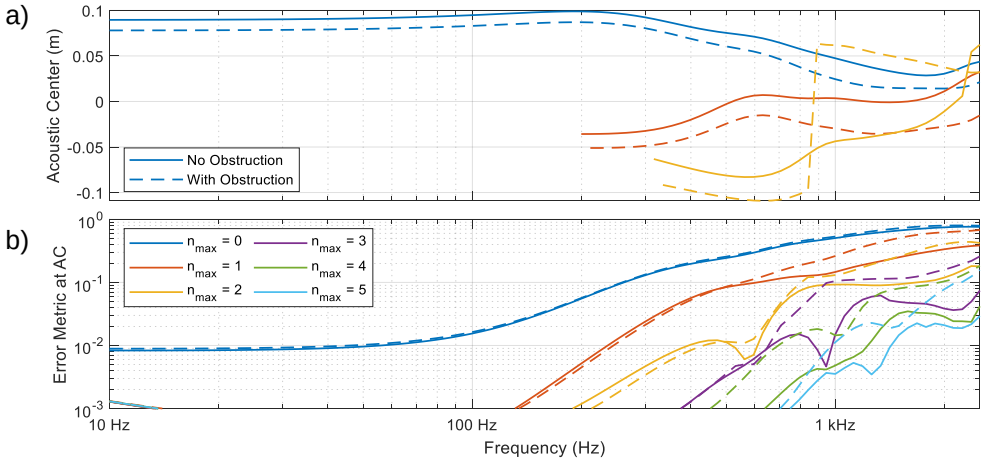

Figure 6: Optimal trial AC (top) and error metric minima (bottom) for the single driver loudspeaker for various reconstruction orders (n), with (solid) and without (dashed) obstacle present.

Figure 7 shows the pressure field from the loudspeaker at 400Hz and 1kHz, with and without the obstruction. These are both above intended the operating frequency of the bass stage but are shown to allow differences to be seen. Optimal zeroth and first order AC positions from fig. 6a are overlaid.

It can be seen that the obstruction's presence has surprisingly little effect at either frequency. At 400Hz there is almost no discernible change except for a slight movement in the pressure null at the top of the figure; this phase lag is likely what has moved the AC downwards. At 1kHz there appears to be greater output from the version with the obstruction, perhaps due to increased radiation impedance (note that a prescribed velocity boundary condition was used in this simulation). Differences are seen in the near field of the obstacle, and a slight focussing effect (Arago spot) is seen above it. It was anticipated that this might move the AC forward, but it has not.

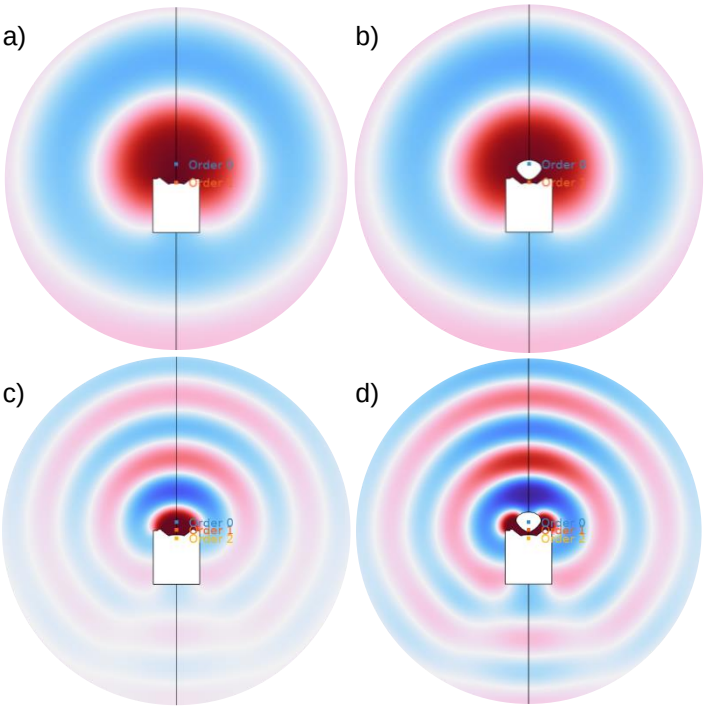

Figure 7: Pressure fields radiated by the single driver loudspeaker at 400Hz (a&b) and 1kHz (c&d), with (b&d) and without (a&c) obstruction, including positions of zeroth (blue) and first (orange) order ACs.

5 OPTIMISATION OF A CARDIOID LOUDSPEAKER

This section presents a model of the full dual driver loudspeaker described in section 1.2 and shown in fig. 1. The geometry is shown in fig. 8. The model of the acoustic exterior is largely unchanged except the maximum element size was doubled to 1.2mm, reducing the $\lambda/5$ frequency to 5kHz. The full 0.6m long loudspeaker is now present, including its rear plate. The front baffle has been moved forward to $z = 0.15\mathrm{m}$ to better position it within the acoustic domain.

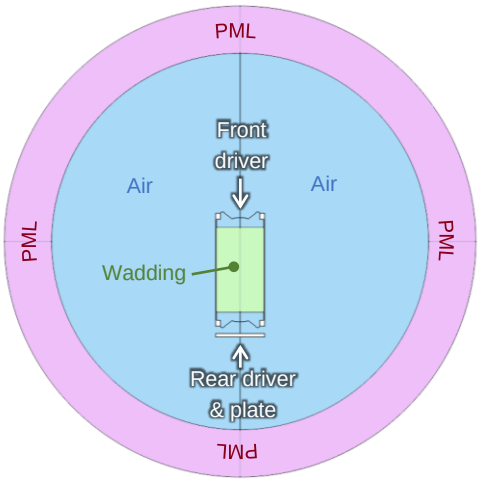

Figure 8: Geometry of dual driver loudspeaker model

A key difference is that the internal air volume of the cabinet is now modelled. The majority of this (green in fig. 8) is filled with wadding material modelled using a Delaney-Bazley model and a flow resistivity of 922 Pa×s/m^2. Also, the two loudspeakers are now coupled to simulated circuits that implement a lumped parameter model of their electroacoustic properties. These use the Thiele-Small values of the drivers used in the prototype. This means that both cones can move when only one driver is driven, an effect that occurs quite strongly at low frequencies in the physical prototype.

The drive signals for the two drivers will be optimised to give the most cardioid directivity possible. Loudspeaker directivity is a function of distance, as discussed earlier. However, it is uncommon to hear distance mentioned in discussion of cardioid directivity, suggesting that this distance-invariant far field model is appropriate:

$$p_{\mathrm{ff}}(\beta, \alpha, \omega) = a_0(\omega) + a_1(\omega)\cos\beta + R_{\mathrm{ff}}(\beta, \alpha, \omega). \quad (13)$$

Here a_0 and a_1 are two frequency-dependent coefficients, the mix of which defines the first-order directivity: $a_1 = 0$ produces an omni-directional pattern, $a_0 = 0$ produces a dipole pattern, or $a_0 = a_1$ produces a cardioid pattern. $R_{\mathrm{ff}}(\beta, \alpha, \omega)$ is the 'residual', meaning any variation in $p_{\mathrm{ff}}(\beta, \alpha, \omega)$ that isn't explained by the first two terms. If the first-order model captures most variation, then this will be small. The search used will find values of a_0 and a_1 while optimising the AC to minimize the norm of R_{ff}.

Noting that $P_0(\cos\beta) = 1$ and $P_1(\cos\beta) = \cos\beta$, as mentioned on page 4, it follows that $a_0(\omega) = d_{0,0}(\omega) \times \sqrt{1/4\pi}$ and $a_1(\omega) = d_{0,1}(\omega) \times \sqrt{3/4\pi}$. If $a_0 = a_1$ then $d_{0,0} = \sqrt{3}d_{0,1}$, so that is the condition that will be solved for. Note that this is very similar to eq. 59 in Bellows and Leishman[2], but the objective there is to find the zeroth-order AC, whereas here it is to optimise for cardioid directivity. Let us define a relative rear gain $\gamma(\omega)$ so total pressure $p(\mathbf{x}, \omega) = p_{\mathrm{front}}(\mathbf{x}, \omega) + \gamma(\omega)p_{\mathrm{rear}}(\mathbf{x}, \omega)$. Noting the linearity of all the operations above, it can be shown that the optimal choice of $\gamma(\omega)$ is:

$$\gamma(\omega) = -\left[d_{0,0,\mathrm{front}}(\omega) - \sqrt{3}d_{0,1,\mathrm{front}}(\omega)\right] / \left[d_{0,0,\mathrm{rear}}(\omega) - \sqrt{3}d_{0,1,\mathrm{rear}}(\omega)\right]. \quad (14)$$

It might be anti-intuitive that far-field directivity would be affected by AC, but the $b_{m,n}$ coefficients have been shown to be, thus the $d_{n,m}$ coefficients defined from them must be too. Considering the form of eq. 11, it seems likely that varying the AC will only cause a phase shift, but this has a significant effect when the result of two drive signals is combined. For $d_{0,0}$ and $d_{0,1}$ alone, a phase shift could be achieved with drive signals. But the approach here also minimises the higher-order residual, which is perhaps its primary achievement. Nonetheless, it is worth noting that this case study transcends the AC definition of Vanderkooy, moving from finding the position where a single-input device is most like a monopole, to finding the AC where a dual-input device can be made most cardioid through DSP.

Figure 9 shows the result of the optimal AC search for the front (solid) and rear (dashed) drivers when driven separately. This is akin to fig. 6 and the error metric is still computed at r_{meas}. The light grey area indicates the space physically occupied by the loudspeaker cabinet. Notably the rear AC is closer to the baffle, presumably due to the presence of the plate. It can be seen from the error metric that both drives naturally exhibit non-monopole behaviour, likely due to the acoustic coupling between the drivers because they are in the same tube. It is around 200Hz that the monopole term explains most of the radiation, and hence the strongest rear drive signal will be required to maintain a cardioid directivity. Higher order terms gradually become significant above 300Hz, but this is above the intended crossover frequency of the design so is not of concern from that perspective. More significantly, there is a jump in the 1st order AC at around 280Hz due to the search space being non-convex. This would require mitigation since discontinuities will be undesirable for drive filter design.

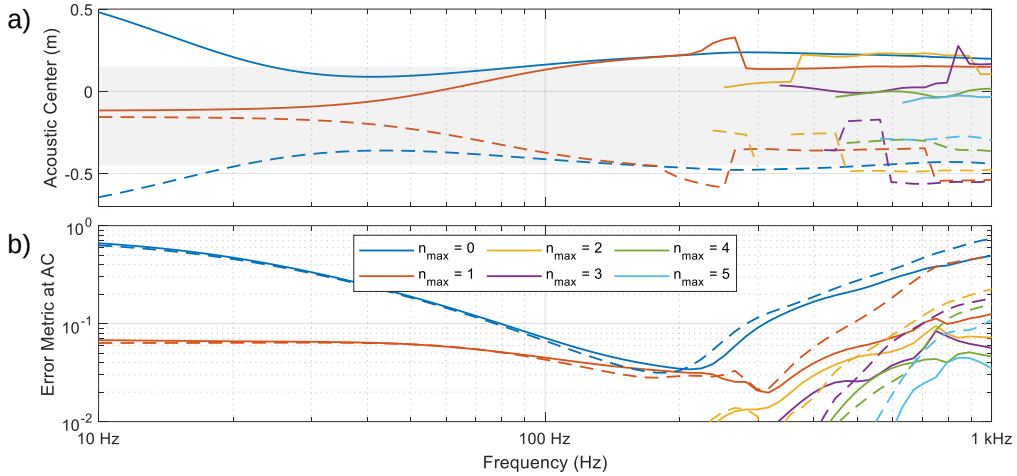

Figure 9: Optimal trial AC (top) and error metric (bottom) for the dual driver loudspeaker for various reconstruction orders (n), for the front (solid) and rear (dashed) drivers driven alone.

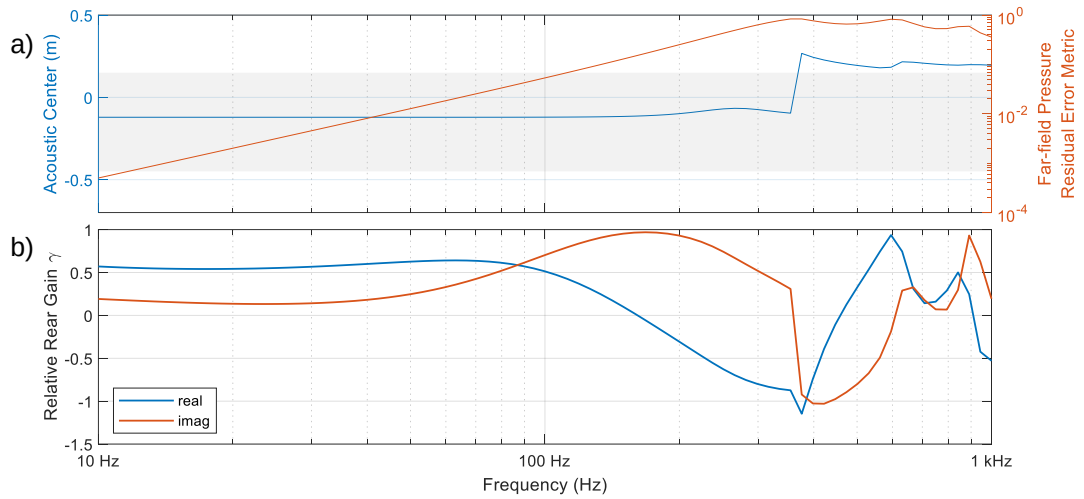

Figure 10: Top: Optimal trial AC (blue, left scale) and far field error metric minima (orange, right scale) for the dual driver loudspeaker when optimised for cardioid directivity.
Bottom: real and imaginary parts of front-to-rear relative gain function to be implemented in DSP.

Figure 10 shows the result of the optimisation process. Metrics here are computed with eq. 12 applied to far-field pressure, as befits the model in eq. 13. The normalised residual (top, orange) starts small at low frequencies but gradually increases to a peak value of 84% at 350Hz. The optimal AC is fairly static at around $-0.11\mathrm{m}$ until that frequency. Plots of the relative rear gain in fig. 10b are smooth and appear suitable for implementation with digital filtering again until 350Hz, where a discontinuity occurs. This artefact is above the intended crossover frequency of the design, however, so is not of significant concern; extrapolation could mitigate for it and produce a smooth target profile for the filter.

Figure 11 shows a polar plot of the far field normalised Sound Pressure Level (SPL) produced post-optimisation. At 50Hz the directivity is extremely close to the ideal cardioid. At 100Hz, a slightly larger deviation occurs, presumably due to a growing quadrupole term. By 316Hz, the higher order terms are significant, and the directivity is clearly no longer cardioid and is polluted by higher order terms. But by this frequency the mid driver will be active also and could be used to optimise directivity too.

6 CONCLUSIONS AND FUTURE WORK

A directional low frequency Acoustic Centre (AC) concept has been proposed and demonstrated with three simulated case studies: one analytical and two numerical concerning loudspeakers. The metrics can be used in a search that identifies the AC for differing orders and frequencies. This was used to optimise cardioid loudspeaker directivity.

Further work is to apply this to non-axisymmetric models and measured data. There is also a need for a process to detect the order of a source as well as its AC. This is challenging to do reliably as the latter varies with the former, and because the search space is often non-convex. But the gains to be had by a directional AC metric are worth this extra effort, in the author's opinion, compared to the – admittedly more elegant – zeroth order AC methods. Achieving synergy with high-frequency AC methods is another long-term goal.

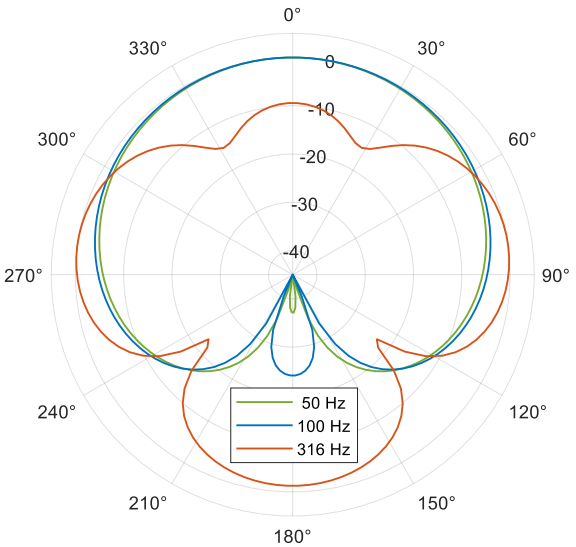

Figure 11: Far field optimised SPL versus angle.

7 ACKNOWLEDGMENTS

The author would like to acknowledge the contribution of the various students who have completed dissertation projects related to the topic of this paper. Although the ideas presented here are entirely the author's own, the momentum created by their efforts, and questions posed by their findings, has assisted in growing this body of research. Notably, Paul Vedier worked on the COMSOL model used in section 5, Alex Booth studied the cardioid optimisation process used in the same section, and Mahmoud Masri studied SH nearfield to far-field transformations. Sean Nielsen, Gabriel Whittle and Dario Niccoli also all undertook projects related to the work herein. Thanks also go to Franz Zotter for pointing the author to a great deal of literature and for providing direct links to some DAGA papers that would otherwise have been difficult to find. And thanks to David Bosch and Jack Oclee-Brown at KEF for providing the loudspeaker drivers used in the prototype loudspeaker that inspired this study.

8 REFERENCES

1. J. Vanderkooy, ‘The Acoustic Center: A New Concept for Loudspeakers at Low Frequencies’, Proc. 121st Aud. Eng. Soc. Conv. (2006).
2. S. D. Bellows and T. W. Leishman, ‘On the low-frequency acoustic center’, J. Acoust. Soc. Am. 153(6) pp3404–3418 (2023).
3. S. Feistel and W. Ahnert, ‘Modeling of Loudspeaker Systems Using High-Resolution Data’, J. Aud. Eng. Soc. 55(7/8) pp 571–597 (2007).
4. J. A. S. Angus, and M. J. Evans, ‘Polar Pattern Measurement and Representation with Surface Spherical Harmonics’, Proc. 104th Aud. Eng. Soc. Conv. (1998).
5. W. Klippel & C. Bellmann, ‘Holographic Nearfield Measurement of Loudspeaker Directivity’, Proc. 141st Aud. Eng. Soc. Conv. (2016)
6. D. Deboy & F. Zotter, ‘Comparison of acoustic centering maps for radiation capture of musical instruments with spherical microphone arrays’, Proc. DAGA (2010) pp 705–706.
7. I. Ben Hagai, M. Pollow, M. Vorländer & B. Rafaely, ‘Acoustic centering of sources measured by surrounding spherical microphone arrays’, J.Acoust.Soc.Am. 130(4) pp2003–2015 (2011)
8. N. R. Shabtai & M. Vorländer, ‘Acoustic centering of sources with high-order radiation patterns’, J. Acoust. Soc. Am. 137(4) pp1947–1961 (2015).
9. J. A. Hargreaves, L. R. Rendell & Y. W. Lam, ‘A framework for auralization of boundary element method simulations including source and receiver directivity’, J. Acoust. Soc. Am. 145(4), pp2625–2637. (2019).
10. M. Melon, C. Langrenne, D. Rousseau, & P. Herzog, ‘Comparison of Four Subwoofer Measurement Techniques’, J. Aud. Eng. Soc. 55(12) pp1077–1091 (2007).
11. W. Ahnert & S. Feistel, ‘The Significance of Phase Data for the Acoustic Prediction of Combinations of Sound Sources’, Proc. 119th Aud. Eng. Soc. Conv. (2005).
12. J. A. Hargreaves & Y. W. Lam, ‘An Energy Interpretation of the Kirchhoff-Helmholtz Boundary Integral Equation and its Application to Sound Field Synthesis’, Acta Acust. u/w Acust. 100(5) pp912–920 (2014).
13. J. A. Hargreaves & Y. W. Lam, ‘Acoustic Cross - Energy Measures and Their Applications’, Proc. 22nd Int. Cong. Sound & Vib. (2015).
14. J. Cheer, ‘Robustness and Efficiency of an Acoustically Coupled Two-Source Superdirective Array’, Proc. 22nd Int. Cong. Sound & Vib. (2015).
15. J. D’Errico, fminsearchbnd https://www.mathworks.com/matlabcentral/fileexchange/8277-fminsearchbnd-fminsearchcon (2012). (Retrieved 4th Oct 2023).